Chemistry–A European Journal
Research Article
doi.org/10.1002/chem.202302497
Chemistry Europe
European Chemical Societies Publishing
www.chemeurj.org

Hexanuclear Ln_6L_6 Complex Formation by Using an Unsymmetric Ligand

Daniel J. Bell,[a] Tongtong Zhang,[a, b] Niklas Geue,[b] Ciarán J. Rogers,[a, c] Perdita E. Barran,[b] Alice M. Bowen,[a, c] Louise S. Natrajan,*[a] and Imogen A. Riddell*[a]

Multinuclear, self-assembled lanthanide complexes present clear opportunities as sensors and imaging agents. Despite the widely acknowledged potential of this class of supramolecule, synthetic and characterization challenges continue to limit systematic studies into their self-assembly restricting the number and variety of lanthanide architectures reported relative to their transition metal counterparts. Here we present the first study evaluating the effect of ligand backbone symmetry on multinuclear lanthanide complex self-assembly. Replacement of a symmetric ethylene linker with an unsymmetric amide at the center of a homoditopic ligand governs formation of an unusual Ln_6L_6 complex with coordinatively unsaturated metal centers. The choice of triflate as a counterion, and the effect of ionic radii are shown to be critical for formation of the Ln_6L_6 complex. The atypical Ln_6L_6 architecture is characterized using a combination of mass spectrometry, luminescence, DOSY NMR and EPR spectroscopy measurements. Luminescence experiments support clear differences between comparable Eu_6L_6 and Eu_2L_3 complexes, with relatively short luminescent lifetimes and low quantum yields observed for the Eu_6L_6 structure indicative of non-radiative decay processes. Synthesis of the Gd_6L_6 analogue allows three distinct Gd···Gd distance measurements to be extracted using homo-RIDME EPR experiments.

Introduction

In recent years significant advances in the synthesis and characterization of self-assembling lanthanide multinuclear architectures[1] have enabled the potential applications of these complexes in imaging,[2] magnetism[3] and sensing[4] to begin to be realized. In particular lanthanide complexes exhibit clear advantages over their transition metal counterparts as they are frequently luminescent,[4a,5] are able to incorporate ancillary ligands that do not bridge between multiple ions,[6] and exhibit fewer restrictions on the coordination number and geometry at the metal sites.[1a,7]

Challenges of rationally designing self-assembling lanthanide complexes and characterizing the often paramagnetic complexes do however continue to limit the number and variety of lanthanide architectures published. In particular, the effect of ligand symmetry on lanthanide complex formation has remained underexplored despite a growing body of work demonstrating that incorporation of reduced symmetry components within transition metal–organic assemblies[8] enables the formation of reduced symmetry binding pockets with the capacity to bind complex guests.[9] In addition, reducing ligand symmetry facilitates the incorporation of more functional groups within a ligand of a given size. Unsymmetric ligands[10] are defined in two classes: i) those incorporating a symmetric backbone and differing in their binding sites (also known as heteroditopic), or ii) those which have equivalent binding sites but an unsymmetric backbone. For lanthanide complexes, research into the formation of helicate structures generated with heteroditopic ligands has enabled controlled self-assembly of bimetallic systems with useful magnetic and imaging properties.[11] The overall architectures formed with the heteroditopic ligands, typically Ln_2L_3 helicates, are however not observed to vary from the structures obtained with the parent homoditopic ligands.

To our knowledge no studies with supramolecular lanthanide complexes have been reported where the removal of symmetry within the spacer backbone has been investigated. Herein we report the formation of an unexpected Ln_6L_6 complex when an unsymmetric ligand (**L1**; Figure 1) is employed in self-assembly reactions with lanthanide triflates of appropriate ionic radii. By contrast, utilizing a symmetrical ligand (**L2**) of

[a] Dr. D. J. Bell, T. Zhang, C. J. Rogers, Dr. A. M. Bowen, Dr. L. S. Natrajan, Dr. I. A. Riddell
Department of Chemistry
University of Manchester
Oxford Road, Manchester, M13 9PL (UK)
E-mail: louise.natrajan@manchester.ac.uk
imogen.riddell@manchester.ac.uk

[b] T. Zhang, N. Geue, Prof. P. E. Barran
Michael Barber Centre for Collaborative Mass Spectrometry
Department of Chemistry
The University of Manchester
131 Princess Street, Manchester, M17DN (UK)

[c] C. J. Rogers, Dr. A. M. Bowen
National Research Facility for Electron Paramagnetic Resonance
Photon Science Institute
The University of Manchester
Oxford Road, Manchester, M13 9PL (UK)

Supporting information for this article is available on the WWW under https://doi.org/10.1002/chem.202302497

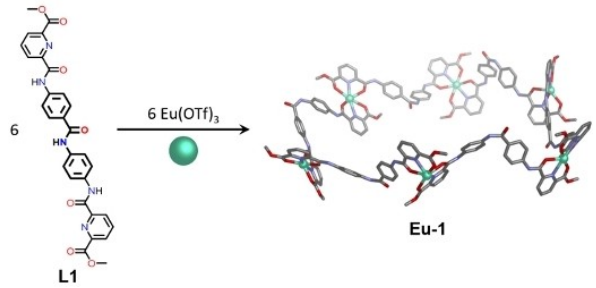

Figure 1. Synthesis of Eu_6L_6 circular helicate (**Eu**–**1**) from **L1** and europium(III) triflate. The highest symmetry isomer of **Eu**–**1** is shown for simplicity, however, NMR analysis indicates a mixture of isomers coexist in solution (Supporting Information S4.2). The Eu_6L_6 model was generated using *Avogadro*[12] and does not include counterions or solvent molecules.

comparable length with equivalent binding sites generates well-recognized Ln_2L_3 and Ln_4L_6 complexes. The hexanuclear architectures are characterized using a combination of NMR, ion mobility mass spectrometry, luminescence and EPR techniques, and their luminescence properties differ from those observed with the Ln_2L_3 and Ln_4L_6 complexes due to their differing coordination environments.

Results and Discussion

A new unsymmetric *bis*tridentate ligand (**L1**; Figure 1) was synthesized via the amide condensation of 4,4′-diaminobenzanilide and the acid chloride of dipicolinate methyl ester. Ligand **L1** incorporates a central amide moiety that reduces the overall symmetry of the molecule compared with classical homoditopic ligands, which commonly display C_2-symmetry. The central amide moiety thus introduces the possibility for isomer formation in multinuclear species, where the ligands may be arranged in a head-to-head or a head-to-tail configuration.[11] The amide functionality also provides potential opportunities for hydrogen bonding[13] to guest molecules or adjacent ligands. Based on previously reported work we hypothesize that three equivalents of ligand could be combined with two equivalents of lanthanide metal salt to generate common supramolecular architectures including Ln_2L_3 helicates[14] and Ln_4L_6 tetrahedra.[4a,15] Initial mass spectrometry studies supported formation of a multinuclear species with a 1:1 ratio of Eu(III) metal ions to ligand, inconsistent with our initial hypothesis that triple helicate or tetrahedral structures would form. Subsequent characterization supported the formation of a Ln_6L_6 circular helicate complex (**1**; Figure 1) in the presence of Eu(III) ions and revealed the effect of lanthanide ionic radius on the outcome of the self-assembly reactions.

Characterisation of unexpected Eu_6L_6 complex

Self-assembly reactions performed in acetonitrile at 333 K with two equivalents of europium(III) triflate and three equivalents of ligand generated a complex, broadened ^{1}H NMR spectrum consistent with the coordination of paramagnetic europium ions to **L1**. By contrast, the mass spectrum clearly displayed intense peaks for a single multinuclear complex (**Eu**–**1**) with a Eu_6L_6 formula, and ten to fifteen triflate counterions (Figure 2a).

Repeating the self-assembly reaction with a 1:1 Eu:**L1** stoichiometry, reflecting the dominant species observed by mass spectrometry, enabled a better defined ^{1}H NMR profile to be obtained (Figure S10). The number of resonances in the ^{1}H NMR spectrum is suggestive of isomer formation, with isomers possible due to *cis*/*trans* isomerisation of the amide bond as well as head-to-tail coordination isomers[11] arising from the variable orientation the unsymmetric ligand **L1** (Supporting Information S4.2). ^{1}H DOSY NMR analysis of this mixture at 6.02 mM Eu(III) concentration supported formation of a single species with a hydrodynamic radius of 1.52 nm, whilst ^{1}H DOSY NMR spectra collected at higher Eu(III) concentrations suggested a larger hydrodynamic radii (2.97 nm) indicative of aggregate formation, most likely a dimer. By comparison, DOSY analysis of the ligand in the absence of metal ions gave a hydrodynamic radius of the ligand as 0.62 nm (Figure S3).

We next evaluated the role of triflate counterions in the self-assembly reaction. Low temperature ^{19}F NMR spectra (Figure S12) revealed multiple fluorine environments suggestive of coordination of triflate to the europium metal centers. Relative

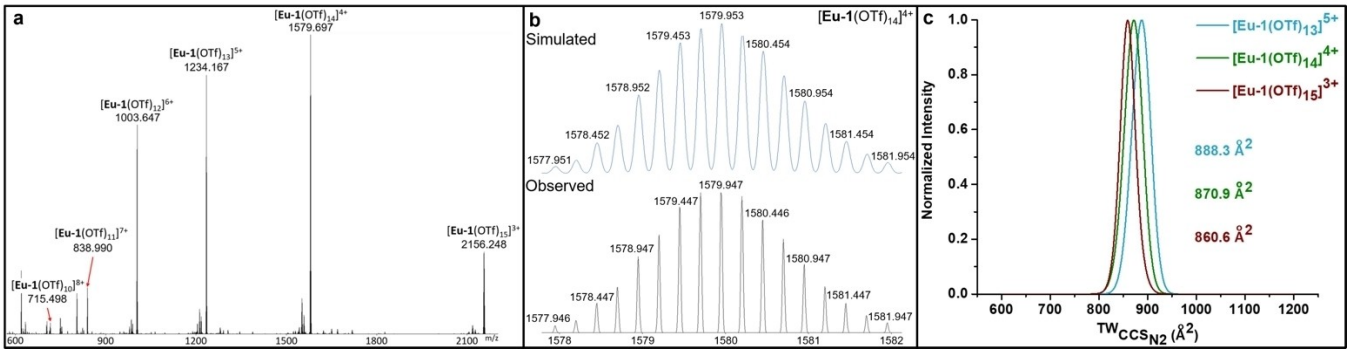

Figure 2. Mass spectra for complex **Eu**–**1**: a) ESI mass spectrum; b) simulated and experimentally observed isotope pattern for [**Eu**–**1**$(OTf)_{14}]^{4+}$; and c) IM–MS data for three **Eu**–**1** cations. For each ion, one $^{TW}CCS_{N2}$ distribution from one data set was fitted to a Gaussian distribution. The ionic diameter calculated from the $^{TW}CCS_{N2}$ measurement is consistent with modelling and DOSY experimental data.

integration of the ^{19}F NMR signals for free and bound triflate supports three triflate ions occupying a unique chemical environment. Self-assembly reactions performed in CD_3CN with $EuCl_3 \cdot 6H_2O$ or $Eu(NO_3)_3 \cdot 5H_2O$ in place of $Eu(OTf)_3$ yielded only insoluble products. Complexation reactions of **L1** and $Eu(OTf)_3$ in the presence of dodecaisopropylbambus[6]uril which is known to bind triflate counterions,[16] also failed to yield soluble products. Together these results support an active role for triflate in the formation of **Eu-1**.[17] We therefore hypothesize that up to three counterions coordinate alongside acetonitrile solvent molecules to fulfill the coordination sphere requirements of the europium(III) ions within the complex. Attempts to observed bound $^{13}CD_3CN$, were inconclusive with no signals consistent with bound solvent observable by ^{13}C NMR spectroscopy (Figure S18); we attribute this to signal broadening upon coordination to the paramagnetic Eu(III) center.

Further support for the proposed Eu_6L_6 circular helicate structure was obtained using ion mobility mass spectrometry (IM–MS), which measures the mass and structure of an analyte in the same experiment.[18] Structural information is provided in form of collisional cross sections (CCS), which correspond to the size and shape of the analyte as well as to the interactions with a neutral buffer gas (here we use nitrogen). Analysis of the different charge states corresponding to complex **Eu–1** indicated that the sequential loss of counterions did not significantly alter the $^{TW}CCS_{N2}$ of the cation (Figure 2c), which suggests a minor impact of the triflate counterions on the overall structure.

Mass to charge peaks corresponding to the cation with three or less triflate ions, which we postulate are coordinated directly to the metal center, were not observed under the conditions of the experiment. $^{TW}CCS_{N2}$ values of **Eu–1** were converted to an ionic diameter of 3.33 nm, based on the assumption of a hard sphere model,[19] which was in good agreement with the hydrodynamic radius calculated by ^1H DOSY NMR spectroscopy (Table S12). Closer examination of the mass spectra also revealed evidence for the formation of aggregates consistent with concentration dependent changes in the hydrodynamic radii observed during DOSY NMR analysis.

Structural models of the proposed circular helicate complex with *cis* and *trans* amide configurations, as well as a linear Eu_6L_6 structure were generated using *Avogadro*[12] (Figure S51). The maximum dimension for each model was measured at 3.8, 4.0 and 6.3 nm for the circular helicate with *cis* amide linkages, *trans* amide linkages and the linear structure, respectively. For both helicate models, the maximal diameter of the model was slightly larger than the experimentally determined diameters obtained by DOSY NMR (3.04 nm) and ion mobility mass spectrometry (3.33 nm), indicating that in solution the helicate may exist in a more closely packed configuration (Table S12). Formation of a catenated structure ($(Eu_3L_3)_2$) could be ruled out on the basis of the collision induced dissociation studies (Figure S48) which indicated fragments of varying sizes were routinely produced and did not show preferential formation of a Eu_3L_3 fragment.[20] Despite exhaustive attempts to isolate crystals of a Ln_6L_6 complex no suitable conditions were found, this we attribute to the presence of a mixture of isomeric species (Supporting Information S4.2) in solution as well as labile Ln–L bonds which were readily disrupted by many of the solvents introduced during attempts to isolate the complex.

Luminescence studies were also undertaken on the reaction mixture in CD_3CN, enabling the determination of the lifetime and quantum yield of Eu_6L_6. Ligand sensitized europium(III) luminescence ($\lambda_{exc} = 330$ nm, $\lambda_{em} = 617$ nm) afforded a typical emission spectrum with four discernable bands corresponding to the ($^5D_0 \rightarrow {}^7F_J$ $J = 0-4$ transitions). The luminescence lifetime recorded at the emission maximum (617 nm) enabled measurement of the luminescence lifetime (τ) as 305 μs and the quantum yield (Φ) was determined as 0.9%. These comparatively low values support our hypothesis that the dipicolinic acid moieties do not fully saturate the lanthanide coordination sphere, and counterions and solvent, which allow for non-radiative decay pathways, are included within the metal coordination sphere.[21]

Effect of lanthanide salt on supramolecular architecture

Following characterization of the Ln_6L_6 structure with europium we sought to explore whether this structure was uniquely formed with europium(III) triflate or if it could be made with alternative lanthanide ions.[22] Mass spectrometric analysis of reaction mixtures generated from 1:1 ratios of lanthanide triflates, where Ln=Sm(III), Tb(III) or Gd(III), and **L1** in acetonitrile supported the formation of Ln_6L_6 complexes in all cases (Figures S22, S24 and S26). For the Sm(III) reaction mixture DOSY NMR confirmed exclusive formation of a single species with a hydrodynamic radius comparable to that reported for the Eu_6L_6 structure under similar conditions (Figure S20). Moreover, pulsed Hahn Echo Detected Field Sweep (EDFS) measurements at 5 K (Figure S53), of the Gd_6L_6 complex (**Gd–1**) displayed broad signals due to a large distributed zero-field splitting (ZFS) parameter indicative of Gd(III) coordination to dipicolinic acid moieties.[23]

To extract inter- spin distance information from the complex, Relaxation Induced Dipolar Modulation Enhancement (RIDME) experiments were performed at Q-band (33.62 GHz) (Figure S55). This single frequency technique is described in detail elsewhere.[24] Homo-spin RIDME has been successfully applied for distance determination in Gd(III) containing complexes,[25] but to our knowledge not yet in systems containing more than two Gd(III) centres. The RIDME measurement of the sample in a mixed solution of CD_3CN:d_8-toluene/ 7:3 (200 μM) after being flash frozen in liquid N_2 and storing at −80 °C gave sharp distances with maxima of 1.5 nm, 2.5 nm and 3.2 nm. These values are consistent with the modelled hexanuclear structure and correlate more closely with the Gd···Gd distances in the model where each of the amide bonds is held in a *cis* configuration (Figure 3).

When the lanthanide triflate was changed to lutetium(III) or ytterbium(III), mass spectrometry revealed mixtures of self-assembled products containing Ln_2L_3 and Ln_4L_6 supramolecular architectures (Figures S31 and S34). These metal to ligand ratios are commonly observed in metal–organic self-assembly reac-

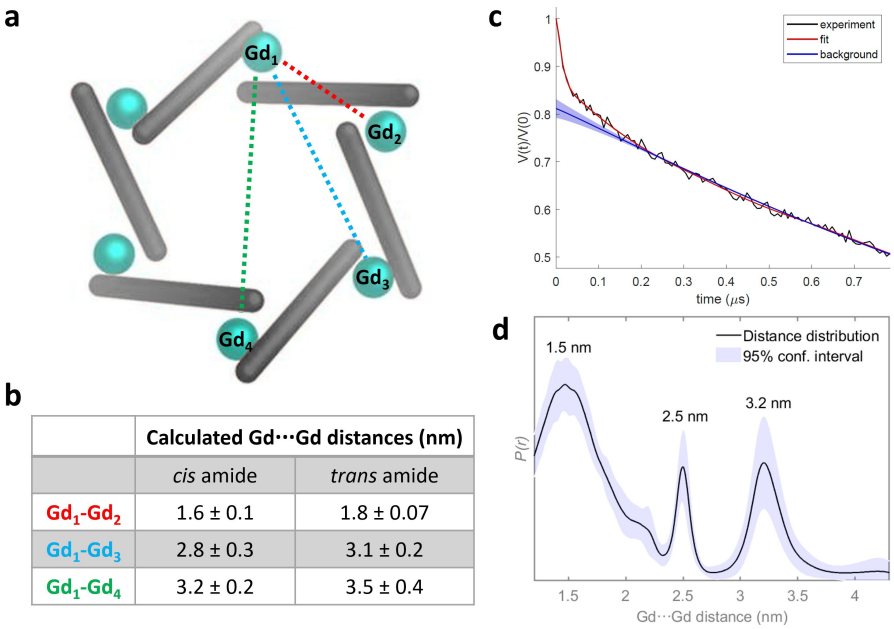

	Calculated Gd···Gd distances (nm)	
	cis amide	*trans* amide
Gd_1-Gd_2	1.6 ± 0.1	1.8 ± 0.07
Gd_1-Gd_3	2.8 ± 0.3	3.1 ± 0.2
Gd_1-Gd_4	3.2 ± 0.2	3.5 ± 0.4

Figure 3. a) Schematic model of M_6L_6 circular helicate indicating the three distinct Gd···Gd distances (Gd_1···G_{d2}, Gd_1···Gd_3 and Gd_1···Gd_4); b) tabulated measurements of distances taken from models generated with *Avogadro*[12] and c) five pulse RIDME trace (black), fit (red) and background (blue) determined by neural network analysis of **Gd-1** after storing at −80 °C, measured at Q-band (33.62 GHz), at a temperature of 5 K with T_{mix} = 100 μs, d) Corresponding distance distribution with 95% confidence interval shown as the blue shaded region, with the maxima of each peak of the distribution annotated.

tions and correspond to triple helicate and tetrahedral architectures, respectively. Both architectures would be expected to incorporate fully saturated metal ion coordination spheres with three tridentate chelates bound at each metal center, and thus would be differentiated from Ln_6L_6 structures by their photophysical properties.

For the mixture generated with lutetium(III) triflate, no evidence for formation of a Lu_6L_6 complex was observed under any conditions. The Lu_2L_3 and Lu_4L_6 complexes were observed to form cleanly by mass spectrometry, whilst ^{1}H NMR spectroscopic analysis of the mixture supported multiple ligand environments consistent with formation of constitutional isomers where each ligand resonance was found in several similar chemical shift environments (Figure S30). The DOSY analysis identified two discrete species with hydrodynamic radii of 1.54 and 1.81 nm which are consistent with Lu_2L_3 and Lu_4L_6 structures, respectively, based on comparison with single-crystal X-ray structures[4a] of structurally related complexes found in the literature. By contrast, mass spectrometry analysis of reaction mixtures generated using ytterbium(III) triflate indicated the mixture consisted of three complexes with Yb_2L_3, Yb_4L_6 and Yb_6L_6 metal:ligand ratios. The ^{1}H NMR spectrum of a mixture generated from a 1:1 combination of $Yb(OTf)_3$ and **L** in acetonitrile indicated multiple peaks across the chemical shift range −30 to 25 ppm (Figure S32).

The observation that Yb(III) and Lu(III) are able to generate the predicted self-assembly products with 2:3 M:L stoichiometry in contrast to reactions performed with Sm(III), Tb(III), Gd(III) and Eu(III) can be rationalized when considering the relative nine coordinate ionic radii of the metal ions.[26] Previous reports[22,27] have highlighted that the ionic radii of lanthanide ions plays a significant role in determining the outcome of supramolecular self-assembly reactions. In this study, nona-coordinated Yb(III) and Lu(III) have the smallest ionic radii (< 110 pm) and are able to accommodate three tridentate binding sites for **L1**. The other cations investigated all have notably larger nine coordinate ionic radii (> 110 pm)[26] and either support formation of a Ln_6L_6 complex, or in the case for La(III) and Nd(III) which have the largest ionic radii, generate featureless spectra and/or precipitate inconsistent with formation of discrete polynuclear species. Reactions with $Y(OTf)_3$, which has an intermediate ionic radius larger than Yb(III) but smaller than Tb(III), also failed to generate discrete complexes (Figure S35).

Role of amide linkage in ligand

We next evaluated the outcome of europium self-assembly reactions with a structurally related ligand (**L2;** Figure 4)) which

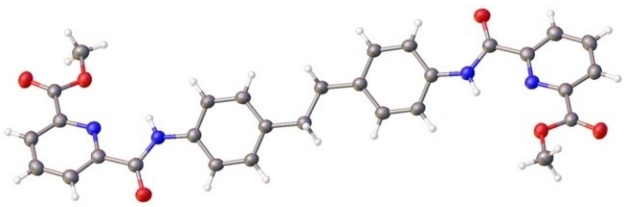

Figure 4. Single crystal X-ray structure[28] of **L2** incorporating a central $-CH_2CH_2-$ linkage in place of the amide (–CONH–) within **L1**.

incorporates a symmetrical ethylene linkage in place of the amide in **L1**.

Ligand **L2** was prepared following a similar synthetic protocol used in the preparation of **L1** and utilized in self-assembly reactions with europium(III) triflate in a 1:1 and 2:3 metal: ligand ratio. Following self-assembly, ^{1}H NMR spectroscopic analysis indicated broadened NMR resonances consistent with coordination of the ligand to the paramagnetic metal centre in both reactions. Closer analysis of the ^{1}H NMR spectra revealed significant differences between the two samples, with more features being observed in the 2:3 metal: ligand ratio reactions. Only one fluorine environment was observed by ^{19}F NMR spectroscopy in both reaction mixtures consistent with bulk triflate anions. Mass spectrometry data for both reaction mixtures also supported different compositions. At 1:1 metal: ligand ratios, signals corresponding to Eu**L2** and Eu_2**L2**$_2$ complexes were identified, whilst 2:3 metal: ligand ratios resulted in observation of Eu_2**L2**$_3$ and Eu_2**L2**$_2$ complexes under comparable measurement conditions. Luminescence measurements of the reaction mixture generated with two equivalents of europium(III) triflate and three equivalents of **L2** supported exclusion of solvent molecules from the inner coordination sphere of the lanthanide ions. Furthermore, significantly longer luminescence lifetimes (1.43 ms) and improved quantum yields of 11% (versus the 0.9% recorded for **Eu**–**1**) were recorded for reaction mixtures generated with europium(III) triflate and **L2**.

The structures observed by mass spectrometry for reactions with **L2** all correspond to low nuclearity ions, indicating that the amide linkage within **L1** is required for formation of the hexanuclear Ln_6L_6 complex. We thus propose that formation of the Ln_6L_6 structure may be governed by the increased rigidity of **L1** versus **L2** which together with the functional groups in the ligand disfavours formation of a close packed Ln_2L_3 helicate.

Conclusions

Exclusive formation of a hexanuclear Ln_6L_6 structure is demonstrated with europium(III), samarium(III), terbium(III) and gadolinium(III) triflate salts. The cationic radius is one determinant of the architecture whilst inclusion of the triflate counterion is also shown to be essential for formation of this structure. Replacement of the central amide moiety in ligand **L1** with a symmetric ethylene bridge generates a second ligand (**L2**) of comparable span to **L1**. Despite the similar ligand parameters and shared metal coordination sites, ligand **L2** does not support formation of the Ln_6L_6 complex indicating that the central moiety influences the outcome of the self-assembled structure. An improved understanding the parameters which govern lanthanide based self-assembly is essential if the full potential of these multinuclear architectures is to be realized. Here, we show how the change in architectural type determined by the cation, anion and ligand can dictate formation of a Eu_6L_6 structure with open coordination sites which detrimentally impacts the luminescence properties of the complex but offers the opportunity for appropriately chosen guest molecules to interact with the supramolecular architecture; work towards this is currently ongoing.

Experimental Section

General Ln_6L_6 self-assembly procedure: **L1** (1 equiv.) and $Ln(OTf)_3$ (1 equiv.) were dissolved in CD_3CN (0.5 mL), resulting in a pale-yellow solution. The solution was sealed in a J-Young NMR tube, and three vacuum/N_2 fill cycles were applied to degas the solution, before being heated (333 K, 24 hr).

Eu_6L1_6 (6.02 mM Eu concentration): ^{19}F NMR(470 MHz, 298 K, CD_3CN): −79.54 (Int = 5), −75.76 (Int = 1) ppm. DOSY diffusion coefficient (CD_3CN, 298 K): 4.309×10^{-10} m^{2}s^{-1}. Accurate mass *m/z*: $[Eu_2\mathbf{L1}_2.(OTf)_2]^{4+}$ = 427.514 (−6.316 ppm), $[Eu_2\mathbf{L1}_2.(OTf)_3]^{3+}$ = 619.002 (−5.816 ppm), $[Eu_6\mathbf{L1}_6.(OTf)_{10}]^{8+}$ = 715.247(−5.173 ppm), $[Eu_2\mathbf{L1}_3.(OTf)_3]^{3+}$ = 804.056 (−4.726 ppm), $[Eu_6\mathbf{L1}_6.(OTf)_{11}]^{7+}$ = 838.990 (−5.006 ppm), $[Eu_6\mathbf{L1}_6.(OTf)_{12}]^{6+}$ = 1003.980 (−5.478 ppm), $[Eu_6\mathbf{L1}_6.(OTf)_{13}]^{5+}$ = 1234.167(−4.537 ppm), $[Eu_6\mathbf{L1}_6.(OTf)_{14}]^{4+}$ = 1579.697 (−4.178 ppm), $[Eu_6\mathbf{L1}_6.(OTf)_{15}]^{3+}$ = 2156.248 (−3.525 ppm).

EuL_2/Eu_2L2_2: **L2**(5.0 mg, 9.28 μmol, 1 equiv.) and $Eu(OTf)_3$ (5.56 mg, 9.28 μmol, 1 equiv.) were dissolved in CD_3CN (0.5 mL), resulting in a pale-yellow solution. The solution was sealed in a J-Young NMR tube and subject to three vacuum/N_2 fill cycles to degas the solution, before being heated (333 K, 24 hr). Accurate mass m/z: $[Eu\mathbf{L2}.(OTf)]^{2+}$ = 420.027 (−5.476 ppm), $[Eu\mathbf{L2}.(OTf)_2]^{+}$ = 989.005 (−5.460 ppm), $[Eu_2\mathbf{L2}_2.(OTf)_4]^{2+}$ = 989.005 (−5.763 ppm)Da.

Eu_2L2_3/Eu_2L2_2: **L2**(5.0 mg, 9.28 μmol, 3 equiv.) and $Eu(OTf)_3$ (3.71 mg, 6.19 μmol, 2 equiv.) were dissolved in CD_3CN (0.5 mL), resulting in a pale-yellow solution. The solution was sealed in a J-Young NMR tube and subject to three vacuum/N_2 fill cycles before being heated (333 K, 24 hr).^{19}F (470 MHz, 298 K, CD_3CN): −79.27 ppm. Accurate mass m/z: $[Eu_2\mathbf{L2}_3.(OTf)]^{5+}$ = 413.468 (−4.595 ppm), $[Eu\mathbf{L2}.(OTf)]^{2+}$ = 420.027 (−5.476 ppm), $[\mathbf{L2}+H]^{+}$ = 539.190 (−5.749 ppm), $[Eu_2\mathbf{L2}_3.(OTf)_2]^{4+}$ = 554.073 (−4.332 ppm), $[Eu\mathbf{L2}_2.(OTf)]^{2+}$ = 689.119 (−4.644 ppm), $[Eu_2\mathbf{L2}_3.(OTf)_3]^{3+}$ = 789.08 (−5.449 ppm), $[Eu\mathbf{L2}.(OTf)_2]^{+}$ = 989.005 (−5.460 ppm), $[Eu_2\mathbf{L2}_2.(OTf)_2]^{2+}$ = 989.005 (−5.763 ppm), $[Eu_2\mathbf{L2}_3.(OTf)_4]^{2+}$ = 1258.098 (−4.690 ppm), $[Eu\mathbf{L2}_2.(OTf)_2]^{+}$ = 1527.190 (−4.125 ppm).

Deposition Number(s) 2291650 (for **L2**) contain(s) the supplementary crystallographic data for this paper. These data are provided free of charge by the joint Cambridge Crystallographic Data Centre and Fachinformationszentrum Karlsruhe Access Structures service.

Acknowledgements

This research was supported by a Royal Society University Research Fellowship (IAR; URF\R1\180414). IAR also acknowledges the EPSRC and the Department of Chemistry at the University of Manchester for a DTG studentship (DJB), and the BBSRC CDT for a studentship awarded to TZ. IAR acknowledges the EPSRC and NMR infrastructure (EP/K039547/1 and EP/R00482X/1). NG is grateful for funding through the President's Doctoral Scholar Award by The University of Manchester. PEB acknowledges the support of EPSRC through the strategic equipment award EP/T019328/1, the European Research Council for funding the MS SPIDOC H2020-FETOPEN-1-2016-2017-801406 and Waters Corporation for their continued support of mass spectrometry research within the Michael Barber Centre

for Collaborative Mass Spectrometry. AMB is grateful to The Royal Society and EPSRC for a Dorothy Hodgkin Fellowship (DH160004), and the University of Manchester for a Dame Kathleen Ollerenshaw Fellowship. AMB. and CJR thank The Royal Society for the Enhancement Award (RGF\EA\180287) which funded the doctoral studentship for CJR. AMB acknowledges the EPSRC funded National Research facility at the University of Manchester (EP/W014521/1, NS/A000055/1, EP/V035231/1 and EP/S033181/1), for use of facility access and support.

Conflict of Interests

The authors declare no conflict of interest.

Data Availability Statement

The data that support the findings of this study are available in the supplementary material of this article.

Keywords: lanthanide · luminescence · polynuclear · self-assembly · unsymmetric ligand

[1] a) D. J. Bell, L. S. Natrajan, I. A. Riddell, *Coord. Chem. Rev.* **2022**, *472*, 214786; b) X.-Z. Li, C.-B. Tian, Q.-F. Sun, *Chem. Rev.* **2022**, *122*, 6374–6458.
[2] a) Z. Wang, L. He, B. Liu, L.-P. Zhou, L.-X. Cai, S.-J. Hu, X.-Z. Li, Z. Li, T. Chen, X. Li, Q.-F. Sun, *J. Am. Chem. Soc.* **2020**, *142*, 16409–16419; b) C. D. B. Vandevyver, A.-S. Chauvin, S. Comby, J.-C. G. Bünzli, *Chem. Commun.* **2007**, 1716–1718.
[3] a) A. Malviya, H. S. Jena, A. K. Mondal, S. Konar, *Eur. J. Inorg. Chem.* **2015**, *2015*, 2901–2907; b) J. Lu, V. Montigaud, O. Cador, J. Wu, L. Zhao, X.-L. Li, M. Guo, B. Le Guennic, J. Tang, *Inorg. Chem.* **2019**, *58*, 11903–11911; c) Y. Zhang, B. Ali, J. Wu, M. Guo, Y. Yu, Z. Liu, J. Tang, *Inorg. Chem.* **2019**, *58*, 3167–3174.
[4] a) X.-Z. Li, L.-P. Zhou, L.-L. Yan, D.-Q. Yuan, C.-S. Lin, Q.-F. Sun, *J. Am. Chem. Soc.* **2017**, *139*, 8237–8244; b) X.-Z. Li, L.-P. Zhou, S.-J. Hu, L.-X. Cai, X.-Q. Guo, Z. Wang, Q.-F. Sun, *Chem. Commun.* **2020**, *56*, 4416–4419.
[5] H.-Y. Wong, W.-S. Lo, K.-H. Yim, G.-L. Law, *Chem* **2019**, *5*, 3058–3095.
[6] a) D. Guo, C.-Y. Duan, F. Lu, Y. Hasegawa, Q.-J. Meng, S. Yanagida, *Chem. Commun.* **2004**, 1486–1487; b) Y. Zhou, H. Li, T. Zhu, T. Gao, P. Yan, *J. Am. Chem. Soc.* **2019**, *141*, 19634–19643.
[7] J.-C. G. Bünzli, *J. Coord. Chem.* **2014**, *67*, 3706–3733.
[8] J. E. M. Lewis, A. Tarzia, A. J. P. White, K. E. Jelfs, *Chem. Sci.* **2020**, *11*, 677–683.
[9] J. E. M. Lewis, J. D. Crowley, *ChemPlusChem* **2020**, *85*, 815–827.
[10] D. Tripathy, N. B. Debata, K. C. Naik, H. S. Sahoo, *Coord. Chem. Rev.* **2022**, *456*, 214396.
[11] T. B. Jensen, R. Scopelliti, J.-C. G. Bünzli, *Inorg. Chem.* **2006**, *45*, 7806–7814.
[12] a) Avogadro: an open-source molecular builder and visualization tool. Version 1.2.0. http://avogadro.cc/; b) M. D. Hanwell, D. E. Curtis, D. C. Lonie, T. Vandermeersch, E. Zurek, G. R. Hutchison, *J. Cheminformatics* **2012**, *4*, 17.
[13] a) Y. Jiao, H.-y. He, J.-Q. Yin, L. Zhou, C. He, C.-Y. Duan, *Inorg. Chem. Commun.* **2016**, *73*, 129–133; b) J. Zhang, C. He, C. Duan, *Inorg. Chem. Commun.* **2015**, *54*, 41–44; c) S. Yi, V. Brega, B. Captain, A. E. Kaifer, *Chem. Commun.* **2012**, *48*, 10295–10297; d) D. Yang, L. K. S. von Krbek, L. Yu, T. K. Ronson, J. D. Thoburn, J. P. Carpenter, J. L. Greenfield, D. J. Howe, B. Wu, J. R. Nitschke, *Angew. Chem. Int. Ed.* **2021**, *60*, 4485–4490.
[14] M. Elhabiri, J. Hamacek, J. -Claude, G. Bünzli, A.-M. Albrecht-Gary, *Eur. J. Inorg. Chem.* **2004**, *2004*, 51–62.
[15] a) K.-H. Yim, C.-T. Yeung, M. R. Probert, W. T. K. Chan, L. E. Mackenzie, R. Pal, W.-T. Wong, G.-L. Law, *Commun. Chem.* **2021**, *4*, 116; b) C.-T. Yeung, K.-H. Yim, H.-Y. Wong, R. Pal, W.-S. Lo, S.-C. Yan, M. Yee-Man Wong, D. Yufit, D. E. Smiles, L. J. McCormick, S. J. Teat, D. K. Shuh, W.-T. Wong, G.-L. Law, *Nat. Commun.* **2017**, *8*, 1128.
[16] L. Jašíková, M. Rodrigues, J. Lapešová, T. Lízal, V. Šindelář, J. Roithová, *Faraday Discuss.* **2019**, *220*, 58–70.
[17] J.-F. Lemonnier, L. Guénée, G. Bernardinelli, J.-F. Vigier, B. Bocquet, C. Piguet, *Inorg. Chem.* **2010**, *49*, 1252–1265.
[18] a) V. Gabelica, A. A. Shvartsburg, C. Afonso, P. Barran, J. L. P. Benesch, C. Bleiholder, M. T. Bowers, A. Bilbao, M. F. Bush, J. L. Campbell, I. D. G. Campuzano, T. Causon, B. H. Clowers, C. S. Creaser, E. De Pauw, J. Far, F. Fernandez-Lima, J. C. Fjeldsted, K. Giles, M. Groessl, C. J. Hogan Jr, S. Hann, H. I. Kim, R. T. Kurulugama, J. C. May, J. A. McLean, K. Pagel, K. Richardson, M. E. Ridgeway, F. Rosu, F. Sobott, K. Thalassinos, S. J. Valentine, T. Wyttenbach, *Mass Spectrom. Rev.* **2019**, *38*, 291–320; b) E. Christofi, P. Barran, *Chem. Rev.* **2023**, *123*, 2902–2949; c) N. Geue, R. E. P. Winpenny, P. E. Barran, *Chem. Soc. Rev.* **2022**, *51*, 8–27.
[19] a) P. Bonakdarzadeh, F. Topić, E. Kalenius, S. Bhowmik, S. Sato, M. Groessl, R. Knochenmuss, K. Rissanen, *Inorg. Chem.* **2015**, *54*, 6055–6061; b) A. Kiesilä, L. Kivijärvi, N. K. Beyeh, J. O. Moilanen, M. Groessl, T. Rothe, S. Götz, F. Topić, K. Rissanen, A. Lützen, E. Kalenius, *Angew. Chem. Int. Ed.* **2017**, *56*, 10942–10946.
[20] A. Kruve, K. Caprice, R. Lavendomme, J. M. Wollschläger, S. Schoder, H. V. Schröder, J. R. Nitschke, F. B. L. Cougnon, C. A. Schalley, *Angew. Chem. Int. Ed.* **2019**, *58*, 11324–11328.
[21] S. W. Magennis, S. Parsons, Z. Pikramenou, *Chem. Eur. J.* **2002**, *8*, 5761–5771.
[22] K.-H. Yim, C.-T. Yeung, H.-Y. Wong, G.-L. Law, *Inorg. Chem. Front.* **2021**, *8*, 2952–2964.
[23] M. Gordon-Grossman, I. Kaminker, Y. Gofman, Y. Shai, D. Goldfarb, *Phys. Chem. Chem. Phys.* **2011**, *13*, 10771–10780.
[24] S. Milikisyants, F. Scarpelli, M. G. Finiguerra, M. Ubbink, M. Huber, *J. Magn. Reson.* **2009**, *201*, 48–56.
[25] a) S. Razzaghi, M. Qi, A. I. Nalepa, A. Godt, G. Jeschke, A. Savitsky, M. Yulikov, *J. Phys. Chem. Lett.* **2014**, *5*, 3970–3975; b) A. Collauto, V. Frydman, M. D. Lee, E. H. Abdelkader, A. Feintuch, J. D. Swarbrick, B. Graham, G. Otting, D. Goldfarb, *Phys. Chem. Chem. Phys.* **2016**, *18*, 19037–19049; c) M. Azarkh, A. Bieber, M. Qi, J. W. A. Fischer, M. Yulikov, A. Godt, M. Drescher, *J. Phys. Chem. Lett.* **2019**, *10*, 1477–1481.
[26] R. D. Shannon, *Acta Cryst. A32* **1976**, 751–767.
[27] a) G. Li, X. Zhao, Q. Han, L. Wang, W. Liu, *Dalton Trans.* **2020**, *49*, 10120–10126; b) A. McRobbie, A. R. Sarwar, S. Yeninas, H. Nowell, M. L. Baker, D. Allan, M. Luban, C. A. Muryn, R. G. Pritchard, R. Prozorov, G. A. Timco, F. Tuna, G. F. S. Whitehead, R. E. P. Winpenny, *Chem. Commun.* **2011**, *47*, 6251–6253.
[28] Deposition Number 2291650 (for **L2**), contains the supplementary crystallographic data for this paper. These data are provided free of charge by the joint Cambridge Crystallographic Data Centre and Fachinformationszentrum Karlsruhe Structures service.

Manuscript received: August 1, 2023
Accepted manuscript online: September 21, 2023
Version of record online: October 31, 2023